
Article:
López-Vaca, R., Narváez-Tovar, C.A., Das, R. et al. (4 more authors) (2025) Mechanobiological Model of Endochondral Ossification and Trabecular Bone Modeling. International Journal for Numerical Methods in Biomedical Engineering, 41 (3). e70024. ISSN 2040-7939

https://doi.org/10.1002/cnm.70024

MECHANOBIOLOGICAL MODEL OF ENDOCHONDRAL OSSIFICATION AND TRABECULAR BONE MODELING.

Rodrigo López-Vaca[1], Carlos A. Narváez[2], Raj Das[3], Gregory de Boer[4], Salah Ramtani[5], Abdelkader Boucetta[6], Diego A. Garzón-Alvarado[2]

[1] **Universidad Santo Tomás – Colombia**
Grupo de estudios y aplicaciones en ingeniería Mecánica (GEAMEC)
oscarlopez@usta.edu.co

[2] **Universidad Nacional de Colombia**
Engineering Modeling and Numerical Methods Group
canarvaezt@unal.edu.co
dagarzona@unal.edu.co

[3] **Centre for Innovative Structures and Materials, School of Engineering**
RMIT University, Melbourne 3001, Australia.
raj.das@rmit.edu.au

[4] **School of Mechanical Engineering, University of Leeds**
G.N.deBoer@leeds.ac.uk

[5] **Université Sorbonne Paris Nord, Laboratoire CSPBAT, équipe LBPS, CNRS (UMR 7244), Institut Galilée, F93430, Villetaneuse, France**

[6] **French National Centre for Scientific Research**

Key words: *Mechanobiology; Bone modeling; Bone remodeling; endochondral ossification*

ABSTRACT

This work presents the integration of mechanobiological models to predict the natural evolution of bone modeling and remodeling processes to obtain the architecture of trabecular bone from the embryonic stage in mammalians. Bone modeling is simulated in two and three dimensions using a reaction-diffusion mechanism with parameters in Turing space. This approach involves the interaction of two molecular factors (VEGF and MMP13) released by hypertrophic chondrocytes that diffuse and interact within a hyaline cartilage matrix. The bone remodeling process follows the model proposed by Komarova et al., employing a set of differential equations to describe autocrine and paracrine interactions between osteoblastic and osteoclastic cells, determining cellular dynamics and changes in bone mass. Bidimensional and tridimensional results for a cartilage portion predict morphological self-organization parameters between VEGF and MMP13, similar to those present in the architecture of immature trabecular bone. These findings suggest that the dynamic properties of molecular factors play a crucial role in the temporal self-organization of bone mineralization metabolism, leading to a heterogeneous trabecular architecture characteristic of primary trabecular bone. Through the three-dimensional bone remodeling model performed on the surface of trabeculae, it is established that equilibrium in population dynamics leads to asynchronous homeostatic remodeling for bone renewal, culminating in the formation of secondary trabecular bone.

1.0 INTRODUCTION

The development of morphology and the mechanical adaptation of immature trabecular bone (bone modeling) are carried out through endochondral ossification. In this complex and not fully understood process, an embryonic cartilage mold is gradually replaced by bone tissue, contributing to its longitudinal growth [1], [2]. Cartilaginous cells undergo differentiation, hypertrophy, and apoptosis during endochondral ossification. Additionally, blood vessels invade the growth cartilage from the ossification zone of the growth plate, facilitating essential processes that supply nutrients and oxygen. As a result, cartilaginous cells (hypertrophic chondrocytes) die, and interstitial tissue is replaced with bone tissue. Ultimately, the calcified cartilaginous matrix transforms into the primary spongiosa, the initial stage of bone formation [3]. The primary spongiosa consists of calcified cartilage located in the ossification zone of the growth plate. Osteoblasts begin depositing osteoid concentrically around the invading blood vessels, forming the first true bony trabeculae, the secondary spongiosa, while chondroclasts resorb the primary spongiosa. This new bone, in turn, is modified by the combined action of osteoclasts and osteoblasts through modeling and remodeling processes to form mature trabeculae. In the process of cartilage matrix ossification, sequential changes in cartilaginous cells are highly regulated by the secretion or production of different systemic and local factors, which regulate the behavior of these cells in the growth cartilage and cells such as osteoblasts and osteoclasts in the calcified matrix [4], [5], [6]. The relationship between molecular factors and their influence on trabecular bone production has yet to be fully understood [7], [8], as well as the presence of certain morphological patterns that give rise to the architecture of immature trabecular bone in mammalians.

Once the bone tissue is formed, it is continuously remodeled throughout life. Bone achieves its increase in size and shape through growth and subsequent modeling [9]. From the point of view of computational biomechanics, several works have developed models to explain and understand this process entirely [10], [11], [12], [13]. Bone modeling is defined as the ability of bone tissue to adapt to mechanical loads caused by continuous bone resorption and formation. It is most noticeable during growth and development and primarily serves to shape and reshape the bone or change the position of its surface related to its central axis. If this process co-occurs at different points, the morphology of the bone can be altered. Resorption and formation are closely linked during bone remodeling, occurring sequentially at the same site. In contrast, during bone modeling, resorption and formation can occur independently, either separately or simultaneously at different locations [14], [15].

According to the above, this article introduces a mathematical model describing the embryonic process of bone production and its subsequent remodeling. The modeling starts from a cartilage matrix that progresses to woven bone, and it is based on two biological processes: endochondral ossification and bone modeling and remodeling. In the first stage, the proposed endochondral ossification model is a biochemical framework governed by a reaction-diffusion (R-D) system with instabilities in Turing space that seeks to elucidate the formation of patterns that give rise to the morphology of the primary spongiosa. The hypothesis for this mathematical model suggests that the development of trabecular bone architecture arises from the interaction of two vital molecular factors secreted during the hypertrophic state of cartilaginous cells that interact by employing the R-D mechanism. These molecular factors carry out processes of degradation of the cartilaginous extracellular matrix and calcification of the remaining cartilage matrix, producing the architecture

of immature bone. Following the model of endochondral ossification, the second stage, the bone remodeling model, is presented, which aims to transform the woven bone into a lamellar bone, maintain homeostatic mineralization and the structural function of the skeletal system by repairing microdamage and adapting the trabecular structure according to biological demands and mechanical stimuli. The remodeling process in this study is governed by the model proposed by Komarova et al. [11], where a set of differential equations relating autocrine and paracrine interactions in perfect equilibrium between osteoblastic and osteoclastic cells determines cellular dynamics and changes in bone mass. It occurs asynchronously and on the surface of ossified trabeculae.

This mathematical model provides a foundational understanding of early trabecular formation and ossification in embryonic processes. Its primary goal is to replicate early-stage ossification, serving as a crucial starting point for understanding the complex mechanisms in early bone development. While shedding light on these processes, the paper prompts inquiries into the diverse molecules involved in prenatal ossification. Despite some open-ended aspects, this work marks a pioneering step toward comprehending the physiological events governing early bone formation. Beyond its scientific implications, the model is a practical tool for scientists, modelers, and healthcare professionals. It encourages further exploration, generating new ideas to advance understanding of the presented hypothesis.

1.1 Endochondral Ossification Model

In his work “The chemical basis of Morphogenesis” [16], Turing suggested that different chemical substances can react and diffuse to produce a heterogeneous spatial pattern in a steady state under certain conditions. From this point of view, biological models described by reaction-diffusion equations with instabilities in Turing space can form patterns that define the morphology of the primary spongiosa [17]. The general equation governing the reaction-diffusion mechanism takes the form of equation (1).

$$\frac{\partial \mathbf{c}}{\partial t} = \gamma \mathbf{f}(\mathbf{c}) + D\nabla^2 \mathbf{c} \tag{1}$$

Where $\mathbf{c}$ is the morphogen concentration vector, t denotes the time, $\mathbf{f}$ represents the kinetic reaction, and D is the diagonal matrix of positive constant diffusion coefficients, γ represents the relative strength of the reaction terms, indicating that an increase in γ can represent an increase in the speed of a reaction step. The models proposed in this work are related to two-species chemical models, $A(\mathbf{x}, t)$ and $B(\mathbf{x}, t)$, where A and B represent the concentrations of the chemical substances at spatial position $\mathbf{x}$ and time t. The boundary conditions for these models are typically zero flux. These models are represented by the system of equations (equation 2), given by:

$$\frac{\partial A}{\partial t} = \gamma F(A, B) + D\nabla^2 A \tag{2a}$$

$$\frac{\partial B}{\partial t} = \gamma G(A, B) + D\nabla^2 B \tag{2b}$$

Where F and G are nonlinear kinetic reaction terms.

Reactive kinetic terms that satisfy the conditions of Turing instability and the diffusion process allow for the generation of time-stable and space-unstable patterns. Extensive research efforts have been focused on the investigation of kinetic reaction terms based on experimental, theoretical, and hypothetical models [16], [18], [19], [20], [21], [22]. The models used in this work for the reactive terms belong to the category of hypothetical models as they are derived from a series of hypothetically obtained chemical reactions, such as the auto-catalytic trimolecular reactions proposed by Schnakenberg [23], [24] involving two chemicals, as shown in equation (3):

$$X \underset{k_2}{\overset{k_1}{\rightleftharpoons}} A, \quad B \overset{k_3}{\rightarrow} Y, \quad 2X + Y \overset{k_4}{\rightarrow} 3X \tag{3}$$

Based on equation (3) and the law of mass action, which describes the relationship between the concentrations of reactants and products in a chemical reaction at equilibrium and states that the reaction rate is directly proportional to the product of the active concentrations of the reactants, it is possible to write the following equations (4):

$$f(A,B) = k_2[A] - k_1[X] + k_4[X]^2[Y], \qquad g(A,B) = k_3[B] - k_4[X]^2[Y] \tag{4}$$

Where k_1, k_2, k_3 and k_4, are positive constants. Assuming an abundance of concentrations A and B, they can be treated as constants.

Another reactive term for generating morphological patterns is based on the glycolysis reaction, where a glucose molecule is broken down to supply energy to cellular metabolism. The complete model involves several saturation terms, but a simplified model can be derived assuming that the chemical concentrations are far from saturation levels, as shown in equation (5):

$$f(A,B) = k_1[A] - k_2[X] - k_3[Y]^2[X], \qquad g(A,B) = k_2[X] - k_4[Y] + k_3[Y]^2[X] \tag{5}$$

The glycolysis represents a scheme based on real biological reactions, which is used extensively in this work as the base for generating the biological pattern formations.

1.2 Bone Remodeling Model

Woven trabecular bone, also known as primary or immature bone, is a type of bone tissue that forms during the early stages of development [25] [26]. However, this type of bone is not exclusive to early growth; it also forms during the callus stage of fracture repair and in pathological conditions such as bone cancer, including osteosarcoma, Paget's disease, fibrous dysplasia, osteomyelitis and metabolic bone diseases, such as hyperparathyroidism and osteogenesis imperfecta . Woven bone is the result of the complete endochondral process. It has a more disorganized and less structured appearance than lamellar bone, the mature bone tissue [2], [27] [28] [26][29][30]. Over time, woven bone can be remodeled by specialized cells called osteoclasts and osteoblasts. This remodeling process gradually transforms woven bone into lamellar bone, which is mor e organized and mechanically more robust [9]. Woven trabecular bone is an initial framework that provides

structural support during rapid bone growth or repair periods. It later undergoes remodeling to become a more organized and mechanically stable lamellar bone.

Bone remodeling is a complex physiological process that spans multiple spatial and temporal scales and is regulated by hormonal and mechanical signals[9]. Imbalances between bone resorption and formation processes can lead to various pathologies. Different in-silico models have been developed to study the influence of mechanical stimuli on the bone remodeling process, bone diseases, implant-bone interactions, and the effects of treatments on bone pathologies[31], [32], [33]. The bone remodeling process involves multiple bone interactions among different types of cells and cellular factors that respond to various mechanical stimuli and biological conditions to repair bone damage and maintain mineral homeostasis [34].

The bone remodeling mathematical model used in this study was developed by Komarova et al. [35] and is used to facilitate the gradual transformation from woven into lamellar bone. In this model, the interaction between autocrine and paracrine factors, between osteoblasts and osteoclasts, and the evolution of bone mass are represented by a nonlinear system of ordinary differential equations that allows for the calculation of cell population dynamics in a basic multicellular unit (BMU) and changes in bone mass at a discrete site on the bone surface. Komarova's model explicitly involves the population of osteoclasts (x_1), osteoblasts (x_2), and bone mass (Z), with different parameters that model the regulation of paracrine and autocrine factors (g_{ii}). The mathematical remodeling model is presented in the following set of equations:

$$\frac{dx_1}{dt} = \alpha_1 x_1^{g_{11}} x_2^{g_{21}} - \beta_1 x_1 \quad \text{(a)}$$

$$\frac{dx_2}{dt} = \alpha_2 x_1^{g_{12}} x_2^{g_{22}} - \beta_2 x_2 \quad \text{(b)} \qquad (6)$$

$$\frac{dz}{dt} = -k_1 y_1 + k_2 y_2, \text{ where } y_i = \begin{cases} x_i - \bar{x}_i, & if\ x > \bar{x}_i \\ 0, & if\ x \le \bar{x}_i \end{cases}$$

Where α_1 and α_2 represent the differentiation rate of osteoblast and osteoclast precursors, β_i is the rate of bone degradation process for *i* = 1,2. The coefficients g_{11}, g_{22}, g_{12}, and g_{21} describe the effectiveness of autocrine (g_{ii}) and paracrine (g_{ij}) signals regulated by RANK, RANKL, OPG, TGFβ, and other factors. In particular, g_{21} represents the inhibition of osteoclast production by osteoblasts, and g_{12} represents the stimulation of osteoblast production. The exponents g_{ij} are positive except for g_{21}, which functions as a regulator of the paracrine signal. Equations 6a and 6b describe the behavior of bone mass considering the following assumptions: *1.* The populations of osteoblasts and osteoclasts at equilibrium consist of non-active cells capable of participating in signaling. *2.* Higher levels above equilibrium are due to the proliferation and activation of cells. *3.* The bone resorption and formation rates are proportional to the number of active osteoclasts and osteoblasts.

The terms $\bar{x}_i$ represent the equilibrium populations of osteoclasts and osteoblasts, respectively, and z represents bone mass. The equilibrium points of the model are given by:

$$\bar{x}_1 = \left(\frac{\beta_1}{\alpha_1}\right)^{\frac{1-g_{22}}{\gamma}} \left(\frac{\beta_2}{\alpha_2}\right)^{\frac{g_{21}}{\gamma}} \quad (7)$$

$$\bar{x}_2 = \left(\frac{\beta_1}{\alpha_1}\right)^{\frac{g_{12}}{\gamma}} \left(\frac{\beta_2}{\alpha_2}\right)^{\frac{1-g_{11}}{\gamma}} \quad (8)$$

Where $\gamma = g_{12}g_{21} - (1 - g_{11})(1 - g_{22})$. Stability analysis was performed at the equilibrium point by studying the linearization using the Taylor series.

According to the above, during endochondral ossification, hypertrophic chondrocytes undergo hypertrophy and eventually die. Blood vessels, osteoclasts, bone marrow cells, and osteoblasts invade the cartilaginous extracellular matrix constructed by chondrocytes. The osteoblasts deposit bone using the remaining cartilaginous matrix as a scaffold. From this process, the hypothesis of the controlled interaction of two molecular signals that diffuse and chemically react in the cartilaginous extracellular matrix is proposed, leading to the formation of immature trabecular bone from the growth cartilage, similar to previous studies [17]. From a bone and mechanical modeling point of view, the effect of mechanical stimulus on bone remodeling is not included because there is no significant stress on the growing structure at this stage of bone formation. Applying this stimulus will result in bone remodeling at later stages of embryonic development. Consequently, the existence of a reaction-diffusion system involving two key molecules, such as VEGF and MMP13, is assumed, which can lead to a stable pattern in time but unstable in space. These three-dimensional patterns resemble the architecture of trabecular bone that occurs during the endochondral ossification process.

2.0 MATERIALS AND METHODS

The proposed model in this research is outlined in Figure 1. This model consists of two stages according to the biological process of embryonic bone development. The model begins with an initial concentration of substances promoting ossification and a three-dimensional representation of a growth plate cartilage model incorporating a defined number of precursor bone cells. These cells migrate through blood vessels in the metaphysis to reach the ossification zone. The first stage of the model aims to recreate the bone mineralization metabolism associated with a self-organized spatial and temporal system using a reaction-diffusion equations system, considering the kinetic reaction of glycolysis for two substances as a reacting term. The second stage establishes a bone remodeling process based on Komarova's model [35], intending to transform immature bone into lamellar or mature bone. These stages are explained in detail below.

2.1 Description of the Endochondral Ossification Model

The proposed regulatory model for the endochondral ossification process is schematized in Figure 2 and is based on an activator-substrate reaction-diffusion (RD) system [18][21]. This process is modeled considering that the reaction terms (synthesis of soluble extracellular factors) depend on the reactant concentration and hypertrophic chondrocytes in the cartilaginous matrix. Accordingly, the main hypothesis of this work is supported by the idea that the origin of the patterns that give rise to the architecture of trabecular bone could correspond, from a mathematical point of view, to the morphological patterns that arise in Turing space when two chemical reactants interact.

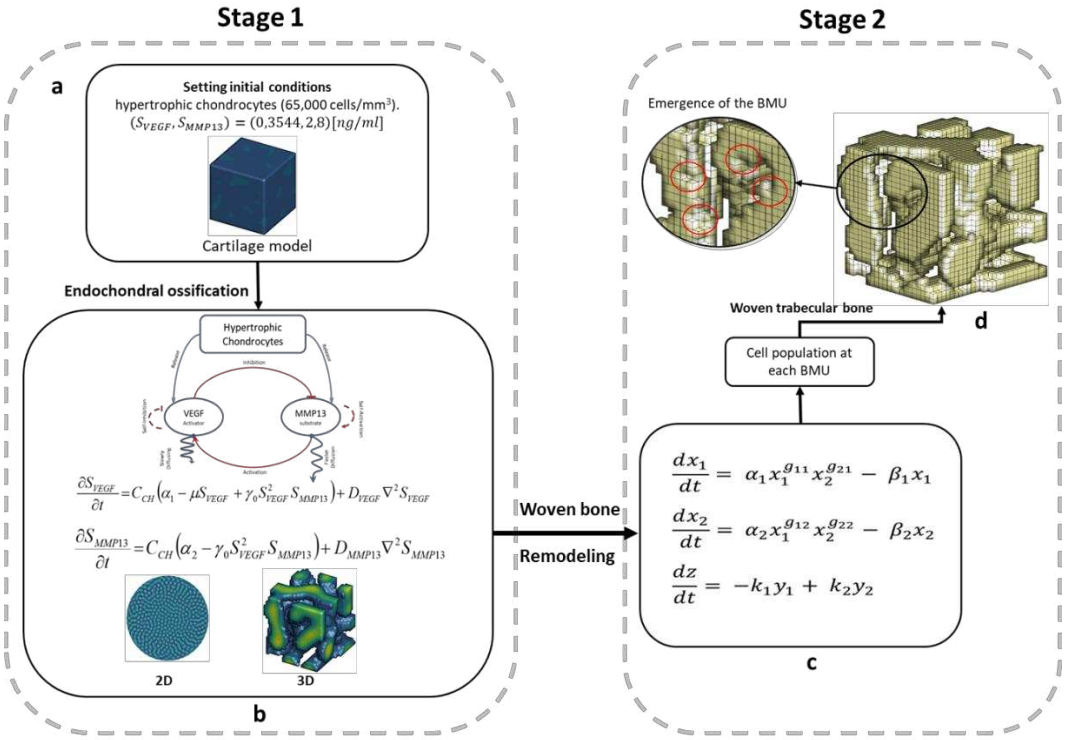

Figure 1. Flow chart of the model coupling endochondral ossification and bone remodeling. Stage 1: bone mineralization metabolism. a. Cubic domain of epiphyseal growth cartilage. b. Endochondral ossification phase. This part of the model employs the regulatory model, the RD equations system, to obtain 2D and 3D results. Stage 2: Bone remodeling process. c. Set of coupled differential equations employed for modeling bone remodeling. d. Woven trabecular bone architecture obtained in stage 1 for the cubic domain. The black circle indicates the interest zone for the remodeling process, and the red circles indicates the potential specific zones where cellular activity can emerge.

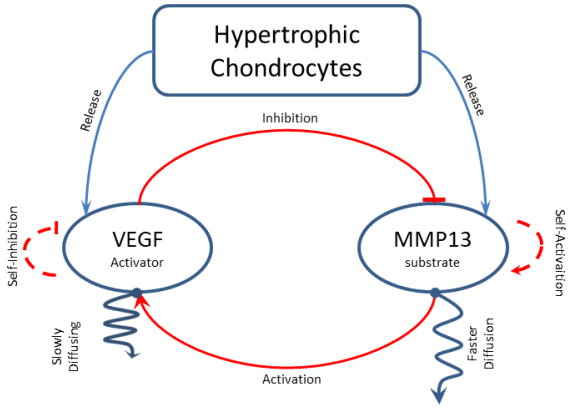

Figure 2. Activator-substrate control system of the molecular process. VEGF: vascular endothelial growth factor, MMP13: matrix metalloproteinase 13. The figure illustrates the relationship of molecular signals produced during the hypertrophic stage of chondrocytes in the growth plate.

According to Figure 2, the regulatory process shows two molecular factors, VEGF (activator) and MMP13 (substrate), released by hypertrophic chondrocytes in the growth plate. These factors diffuse in the cartilaginous matrix and react with each other. The diffusion process in this model is the main agent responsible for producing non-homogeneous spatial instabilities, which lead to the generation of patterns in the endochondral ossification process. The control system derived from the Reaction-Diffusion system indicates that with a low substrate concentration (MMP13), the activator (VEGF) concentration increases, facilitating the invasion of vascular cells and the degradation of the cartilaginous matrix. On the other hand, the control system shows that with the presence of a high concentration of VEGF, the concentration of MMP13 decreases, allowing the invasion of the remaining cartilage by the ossification front, leading to its mineralization and closing the endochondral ossification process.

The processes of self-activation and self-inhibition of the molecular factors present in the control system indicate that near the steady state of the reactants $f(VEGF, MMP13) = 0$, $g(VEGF, MMP13) = 0$, a small increase in the concentration of MMP13 temporarily amplifies its concentration, while small increases in the concentration of VEGF temporarily reduce the production of this factor.

The reaction-diffusion system for the model representing the regulatory process shown in Figure 1 employs the kinetic reaction of glycolysis as a reactive term. Glycolysis is the process of glucose synthesis to provide energy for cellular metabolism. This model can exhibit several phenomena associated with glycolysis and oscillatory behaviors. The kinetic reaction of glycolysis is based on real biological reactions and explains the behavior of an activating chemical in the presence of a substrate chemical [18]. The system of equations (10) can represent this reaction in the immature trabecular bone morphogenesis model.

$$\frac{\partial S_{VEGF}}{\partial t} = C_o\,(\delta - \kappa S_{VEGF} - \gamma_o S_{VEGF} S_{MMP13}^2) + D_{VEGF}\nabla^2 S_{VEGF} \tag{10a}$$

$$\frac{\partial S_{MMP13}}{\partial t} = C_o(\kappa S_{VEGF} - S_{MMP13} + \gamma_o S_{VEGF} S_{MMP13}^2) + D_{MMP13}\nabla^2 S_{MMP13} \tag{10b}$$

$$\frac{\partial c_{Bone}}{\partial t} = \eta \frac{S_{VEGF}^n}{S_{VEGF}^n + S_{umbral}^n} \frac{T_a^r}{T_a^r + t^r} \tag{10c}$$

Where C_o is the concentration of hypertrophic chondrocytes, S_{VEGF} and S_{MMP13} represent the concentrations of the molecular factors VEGF and MMP13, respectively. δ quantifies the initial amount of VEGF due to hypertrophic chondrocytes. κ in equation 10a is a constant that quantifies the consumption of VEGF, and in equation 10b, it quantifies the production of MMP13. γ_0 regulates the nonlinear interaction between the MMP13-VEGF concentration, quantifying the concentration or inhibition of each molecular factor. D_{VEGF} and D_{MMP13} are the diffusion coefficients of VEGF and MMP13, respectively. In the biological interpretation of the equations mentioned above, the term $\gamma_0 S_{VEGF} S_{MMP13}^2$ represents the nonlinear activation of S_{MMP13} (VEGF production due to the presence of MMP13) and the nonlinear consumption of S_{VEGF} (due to the presence of MMP13). Equation (10c) represents the activation of the bone production rate due to high VEGF levels, which are regulated over time. In this equation, c_{Bone} indicates the bone production per unit volume due to the concentration and distribution of VEGF within the domain. η is a constant that regulates bone production over time, S_{umbral}^n represents the value of the VEGF concentration at which the

ossification process begins. T_a is the time required for cartilage calcification and t^r is the time limiting bone production.

The equations (10) were implemented and numerically solved using the finite element method with a Newton-Raphson scheme, as shown in equation 11.

$$\begin{bmatrix} \frac{\partial r^e_{S_{VEGF}}}{\partial \tilde{S}^e_{VEGF}} & \frac{\partial r^e_{S_{VEGF}}}{\partial \tilde{S}^e_{MMP13}} \\ \frac{\partial r^e_{S_{MMP13}}}{\partial \tilde{S}^e_{VEGF}} & \frac{\partial r^e_{S_{MMP13}}}{\partial \tilde{S}^e_{MMP13}} \end{bmatrix} \begin{bmatrix} \Delta S^e_{VEGF} \\ \Delta S^e_{MMP13} \end{bmatrix} = - \begin{bmatrix} r^e_{VEGF} \\ r^e_{MMP13} \end{bmatrix} \tag{11}$$

Where:

$$\frac{\partial r^e_{S_{VEGF}}}{\partial \tilde{S}^e_{VEGF}} = \frac{C_o}{\Delta t} \int_\Omega \boldsymbol{N}^T_{VEGF} \boldsymbol{N}_{VEGF}\, d\Omega + \alpha C_o \left[D_{VEGF} \int_\Omega \nabla \boldsymbol{N}_{VEGF} \nabla \boldsymbol{N}_{VEGF} + \int_\Omega \mathbf{N}^T_{VEGF} \boldsymbol{N}_{VEGF} k d\Omega + \gamma_o \int_\Omega \mathbf{N}^T_{VEGF} \boldsymbol{N}_{VEGF} \left(\boldsymbol{N}_{MMP13}\, \tilde{S}^e_{MMP13} \right)^2 d\Omega \right]^{t+\Delta t}$$

$$\frac{\partial r^e_{S_{VEGF}}}{\partial \tilde{S}^e_{MMP13}} = 2\alpha C_o \gamma_o \left[\int_\Omega \mathbf{N}^T_{VEGF} \boldsymbol{N}_{VEGF}\, \tilde{S}_{VEGF} \boldsymbol{N}_{MMP13} \boldsymbol{N}_{MMP13}\, \tilde{S}^e_{MMP13}\, d\Omega \right]^{t+\Delta t}$$

$$\frac{\partial r^e_{S_{MMP13}}}{\partial \tilde{S}^e_{VEGF}} = \alpha C_o \left[-k \int_\Omega \mathbf{N}^T_{MMP13} \boldsymbol{N}_{VEGF}\, d\Omega - \gamma_o \int_\Omega \mathbf{N}^T_{MMP13} \boldsymbol{N}_{VEGF} \left(\boldsymbol{N}_{MMP13}\, \tilde{S}^e_{MMP13} \right)^2 d\Omega \right]^{t+\Delta t}$$

$$\frac{\partial r^e_{S_{MMP13}}}{\partial \tilde{S}^e_{MMP13}} = \frac{C_o}{\Delta t} \int_\Omega \boldsymbol{N}^T_{MMP13} \boldsymbol{N}_{MMP13}\, d\Omega + \alpha C_o \left[D_{MMP13} \int_\Omega \nabla \boldsymbol{N}_{MMP13} \nabla \boldsymbol{N}_{MMP13} + \int_\Omega \mathbf{N}^T_{MMP13} \boldsymbol{N}_{MMP13} d\Omega - 2\gamma_o \int_\Omega \mathbf{N}^T_{MMP13} \boldsymbol{N}_{VEGF} \boldsymbol{N}_{MMP13} \boldsymbol{N}_{MMP13}\, \tilde{S}^e_{MMP13}\, \tilde{S}^e_{VEGF} d\Omega \right]^{t+\Delta t}$$

$r^e_{S_{VEGF}}$ and $r^e_{S_{MMP13}}$ are the residual vectors for each equation, $\boldsymbol{N}_{VEGF}$ and $\boldsymbol{N}_{MMP13}$ represent the shape function matrices, $\nabla \boldsymbol{N}$ is the gradient vector of the shape functions. $\tilde{S}^e_{MMP13}$ and $\tilde{S}^e_{VEGF}$ are the values of S_{VEGF} and S_{MMP13} at the nodal points. The superscript e indicates the finite element discretization of the variable.

The solution of the system of equations was performed using an incremental, iterative scheme that computationally determines the evolution of both the concentration of the molecular factors (S_{VEGF}, S_{MMP13}) and the production of primary spongy bone.

2.2 Description of the Trabecular Bone Remodeling Model

Once the reaction-diffusion system of equations representing the endochondral ossification process has been solved, a new process governed by the model proposed by Komarova et al. [5] is described. This process is represented by differential equations (1) and (2), which were solved using the fourth-order Runge-Kutta method based on the Taylor series. The coupled system of equations was solved using the following approximation:

$$x_{1_{i+1}} = x_{1_i} + \frac{\Delta t}{6}(k_1 + 2k_2 + 2k_3 + k_4)$$
$$x_{2_{i+1}} = x_{2_i} + \frac{\Delta t}{6}(v_1 + 2v_2 + 2v_3 + v_4) \quad (12)$$

Where Δt refers to the size of the interval when time is discretized, and the variables k_i and v_i are the slope values of the lines used to approximate equations (12) simultaneously. These values are determined using the following expressions:

$$\begin{aligned}
k_1 &= f\left(t_i, x_{1_i}, x_{2_i}\right) \\
v_1 &= g\left(t_i, x_{1_i}, x_{2_i}\right) \\
k_2 &= f\left(t_i + \frac{\Delta t}{2}, x_{1_i} + \frac{\Delta t}{2}k_1, x_{2_i} + \frac{\Delta t}{2}v_1\right) \\
v_2 &= g\left(t_i + \frac{\Delta t}{2}, x_{1_i} + \frac{\Delta t}{2}k_1, x_{2_i} + \frac{\Delta t}{2}v_1\right) \\
k_3 &= f\left(t_i + \frac{\Delta t}{2}, x_{1_i} + \frac{\Delta t}{2}k_2, x_{2_2} + \frac{\Delta t}{2}v_2\right) \\
v_3 &= g\left(t_i + \frac{\Delta t}{2}, x_{1_i} + \frac{\Delta t}{2}k_2, x_{2_i} + \frac{\Delta t}{2}v_2\right) \\
k_4 &= f\left(t_i + \Delta t, x_{1_i} + k_3\Delta t, x_{2_i} + v_3\Delta t\right) \\
v_4 &= g\left(t_i + \Delta t, x_{1_i} + k_3\Delta t, x_{2_i} + v_3\right)
\end{aligned} \quad (13)$$

For trabecular remodeling, according to the approximation equations, the population of osteoclasts (x_1) and osteoblasts (x_2) along with the percentage of mass are determined at each time step Δt. Cellular dynamics variation in the basic multicellular unit (BMU) was implemented randomly and simultaneously on the trabecular surface and in areas representing the occurrence of microdamage or changes in bone density to simulate the homeostatic remodeling process. This activation or deactivation of bone tissue removal and deposition processes is based on changes in the cell population at each Δt, following the model proposed by Komarova.

3.0 RESULTS AND DISCUSSION

3.1 Endochondral Ossification Model

One of the most studied problems in developmental biology is the formation of spatial patterns during embryonic development. Various theories have been proposed to explain this phenomenon, with the most extensively studied being Turing's reaction-diffusion theory [16]. This theory suggests that a chemical pre-pattern is initially established through a reaction-diffusion system of chemical substances, and cells respond to this pre-pattern by differentiating or expressing cell behaviors that give rise to biological structures. In this context, the Turing theory helps explain how patterns and spatial structures arise in various biological phenomena, such as segment formation in embryos, the appearance of spots and stripes on animal skin, the distribution of structures like teeth, the appearance and location of secondary ossification centers [36], the formation of fingerprints [37],

endochondral and intramembranous ossification [17], [38], [39], and the formation of the cerebral cortex during fetal development [40]. In this work, this theory was used to reproduce the architecture of immature trabecular bone based on the spatial organization of molecular factors involved in the ossification and degradation of the cartilaginous matrix through their chemical reaction and diffusion. The generated patterns resemble those present in this tissue.

The models presented and developed here are useful for understanding and studying the biological processes of endochondral ossification and bone remodeling, their natural course, disorders, and pathologies affecting the complex interaction among different cell groups involved in endochondral ossification and bone remodeling.

The presented model predicts the formation of primary trabecular bone through the kinetic reaction between the molecular factors VEGF and MMP13. This reaction exhibits the formation of spatiotemporal patterns that distribute within the cartilage model, leading to its degradation and ossification through the action and interaction of the molecular factors, as observed in Figures 3 and 6.

Initially, the growth plate is assumed to be a structural matrix with an initial concentration of hypertrophic chondrocytes (65,000 cells/mm^3). The initial concentrations of VEGF and MMP13 are randomly distributed within the growth plate, with a perturbation of 10% around the steady-state concentration given by $(S_{VEGF}, S_{MMP13}) = (0{,}3544, 2{,}8)[ng/ml]$ [14]. The selection of random initial conditions around the steady state is similar to the event of molecular expression by hypertrophic chondrocytes in an area where the mineralization process of the cartilaginous matrix will occur. The flow condition for each molecular factor at the boundary is assumed to be zero due to the self-organization of patterns within a specific domain, which is the most important aspect of the proposed system. The last implies that no disturbances should be caused by external flows directed toward the domain under study. The parameters used for the reaction-diffusion system are presented in Table 1.

Parameter	Magnitude	Units
S_{VEGF}	1	ng/ml
S_{MMP13}	1	ng/ml
C_o	$65(10^3)$	$cells/mm^3$
D_{VEGF}	$6{,}9(10^{-5})$	mm^2/s
D_{MMP13}	$5{,}9(10^{-4})$	mm^2/s
δ	$2{,}8$	$mm^3/cells\ day$
κ	$0{,}06$	$mm^3/cells\ day$
γ_o	$1{,}327(10^{12})$	$mm^9/cells\ day\ g^2$

Table 1. General parameters of the endochondral ossification model.

The presented endochondral ossification model has been implemented two and three-dimensionally. Each domain used in the solution represents a portion of bone tissue corresponding to a neonate mammalian at the initial month of age. In the two-dimensional case, a circular domain with a diameter of 8 mm was utilized, roughly corresponding to the radiographic diameter of the ossification core in the femoral epiphysis in neonates. For the analysis, the domain was divided into

3084 quadrilateral elements with four nodes per element and 3136 nodes. The mesh convergence procedure demonstrated that this number of elements is appropriate for the simulation.

Figure 3 presents the results of the 2D numerical simulation of the reaction-diffusion system described in equations (10), considering a time interval of 20 days. This representation shows the diffusion, reaction, and temporal distribution of the molecular factors VEGF (green and yellow areas) and MMP13 (dark blue areas). The distribution produces a macroscopic pattern similar to that found in the primary spongy bone of the ossification core resulting from the endochondral ossification process.

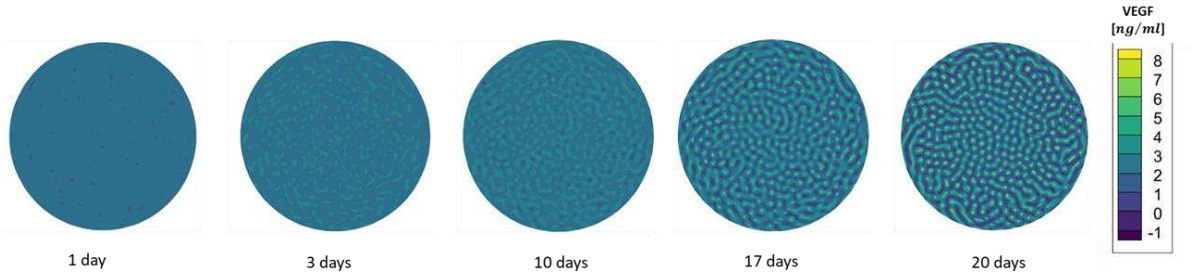

Figure 3. Two-dimensional results of the numerical solution of the R-D system. Temporal evolution of the concentration of molecular factors VEGF (green and yellow areas) and MMP13 (dark blue areas) over a time interval of 1 to 20 days.

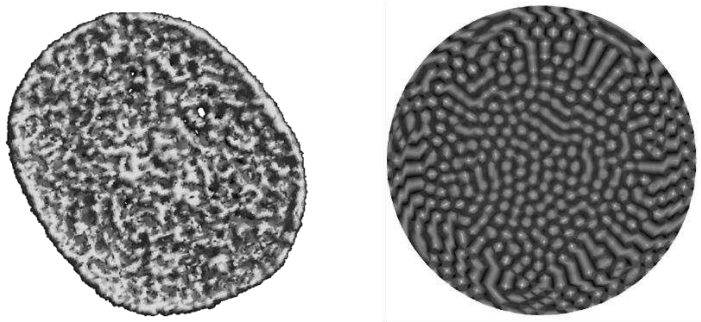

Figure 4. Comparison of 2D dimensional results of the proposed R-D system, the grey areas represent primary trabecular bone formation, and the black areas represent hyaline cartilage degradation. a. Micro-computed tomography cross-section of postnatal mouse femur metaphysis [41]. b. Result obtained from the proposed R-D system using a circumference of 8 mm diameter.

Figure 4 shows the similarities between the morphology of immature trabecular bone in the mouse femur and the spatio-temporal distribution of the R-D model using the molecular factors VEGF and MMP13. The morphology of primary mouse trabecular bone has a characteristic structure of two-dimensional interconnections, with trabeculae arranged in a complex manner and adapted to biological and mechanical demands. In contrast, applying an R-D model with parameters in Turing space, in line with Turing's theory of morphogenesis, reveals an emergent pattern of bone formation that proceeds autonomously and self-organizing. This theoretical model suggests that biochemical processes and signal diffusion play a crucial role in the generation of trabecular architecture.

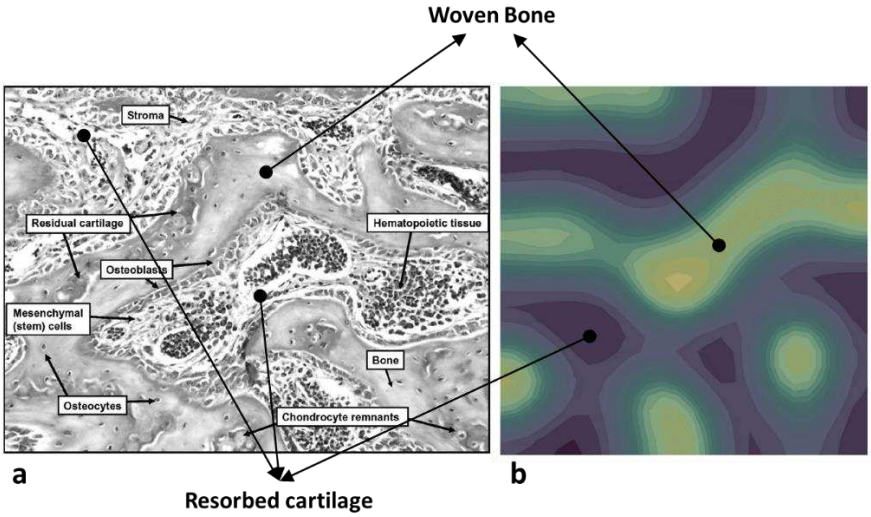

Figure 5. Comparison of the primary spongy bone structure. **(a)** micrograph of turkey bone marrow [42] **(b)** trabecular bone structure obtained using the R-D endochondral ossification model in a 0.46 mm square side.

The interaction between the molecular factors VEGF and MMP13 using the R-D model with reactive terms of glycolysis can be seen in Figure 5b, where the pattern formed from a homogeneous, uniform state faithfully reproduces the morphology of immature trabecular bone. This phenomenon is similar to vertebrate endochondral ossification, as shown in Figure 5a. It should be noted that Figure 5 highlights the process of primary spongy bone formation mediated by the presence of VEGF and the resorption of hyaline cartilage under the influence of MMP13. This interaction results in the configuration of the trabecular structure, which provides a fundamental scaffold for the process of bone remodeling and, therefore, the formation of mature bone.

In the three-dimensional case, the endochondral ossification model was developed in a hexahedral domain with dimensions of 0.46 mm per side. This domain represents a portion of the growth plate in the femoral epiphysis of a gestating mammalian (first month of life) and was discretized into 42875 hexahedral elements and 46456 nodes. For this case, the mesh convergence procedure demonstrated that this number of elements is appropriate for the simulation.

Figure 6 shows the results of the numerical solution of the reaction-diffusion system presented in equations. The chemical interaction of the molecular factors VEGF and MMP13 and their temporal distribution generates patterns that spatially organize themselves, similar to the micro-architecture of the primary trabecular bone.

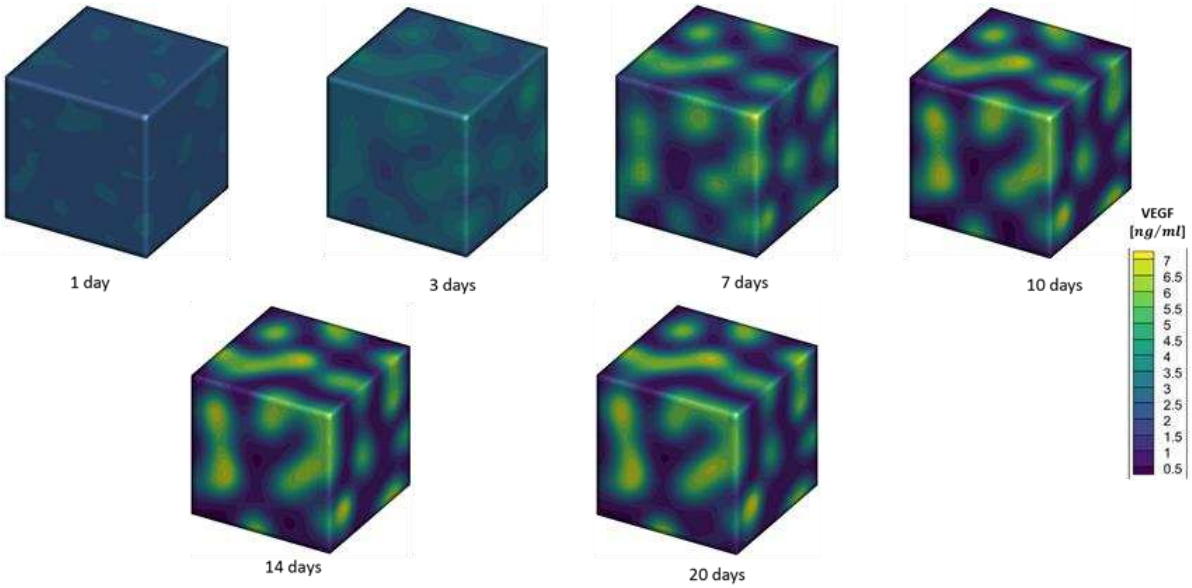

Figure 6. Three-dimensional results of the numerical solution of the R-D system. Temporal evolution of the concentration of molecular factors VEGF (green and yellow areas) and MMP13 (dark blue areas) over a time interval of 1 to 20 days.

Figure 7 shows the temporal cartilage degradation and mineralization process, leading to the ossification process. It can be observed that in areas where the concentration of MMP13 is high (blue zones), the cartilage degrades. In contrast, in areas where the concentration of VEGF is high (green zones), trabecular bone formation occurs, giving rise to the primary trabecular bone.

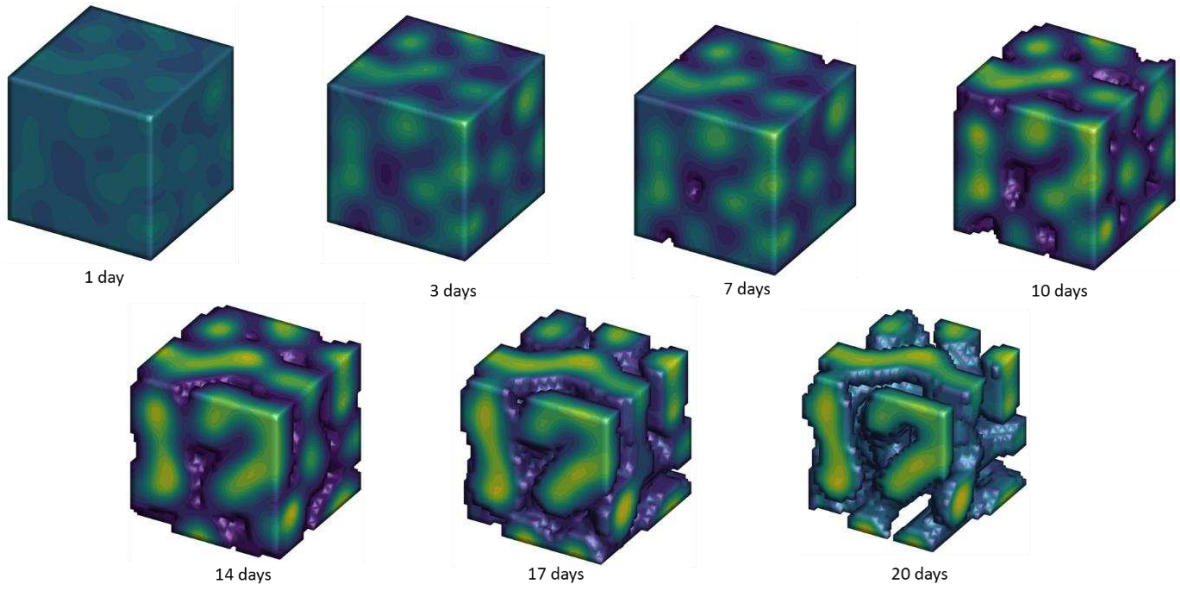

Figure 7. Temporal degradation process of the cartilaginous matrix over a time interval of 1 to 20 days due to the action of MMP13 concentration, resulting from the numerical solution of the R-D system. Dark blue zones represent high MMP13 concentrations, indicating cartilage degradation,

whereas green and yellow zones represent high VEGF concentrations, indicating immature bone formation.

Figure 8 compares the results obtained from the endochondral ossification model and a cubic portion of 5 mm side length of gestating pig bone. It can be observed that the patterns generated by the interaction of molecular factors VEGF and MMP13 through the R-D system faithfully reproduce the architecture of trabecular bone in a cubic space with a side length of 0.46 mm. In this model, the trabeculae exhibit a thickness of 0.13-0.15 mm, similar to what can be measured in the microtomography of pig bone.

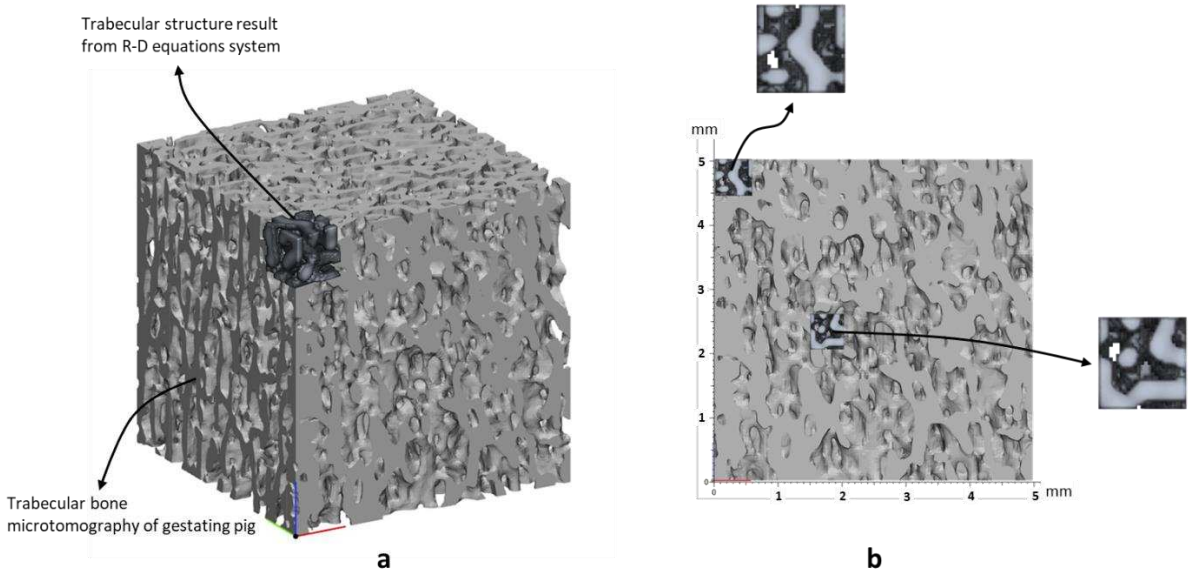

Figure 8. *Validation of R-D Model with Computational Microtomography*. Comparison of R-D model results with computational microtomography of a 5 mm side length portion of trabecular bone from a gestating pig. **a.** *3D visualization*. Superimposition of R-D model result (dark zone) on computational microtomography of gestating pig trabecular bone (5 mm side length). **b**. *2D Frontal View*. Comparison of R-D model result (highlighted zones) with microtomography image of gestating pig trabecular bone portion.

Despite the simplifications used, the presented model of endochondral ossification, governed by the reaction-diffusion equations system with a glycolysis reactive term, accurately reproduces the architecture of immature trabecular bone, evidencing the interaction between molecular factors expressed by chondrocytes in the growth plate: matrix metalloproteinases MMP13 and vascular endothelial growth factor VEGF. In the regulatory model depicted in Figure 2, MMP13 is responsible for the growth plate's degradation. It promotes the activation of VEGF, which accelerates vascularization and initiates mineralization and calcification of the cartilage. However, this process does not solely rely on these molecular factors. Systemic factors such as growth hormone (GH) and thyroid hormone, as well as locally secreted factors like Indian hedgehog (Ihh) and parathyroid hormone-related peptide (PTHrP), fibroblast growth factors, extracellular matrix components, and transcription factors that regulate the gene expression of chondrocytes, such as Runx2, Sox9, and

MEF2C, are involved [1], [4], [28] – [30]. Therefore, the possibility of a new bioregulatory loop, including other molecular factors, cannot be ruled out to develop and control the degradation and ossification process.

3.2 Bone Remodeling Model

In endochondral ossification, immature trabecular or fibrous bone is formed as hyaline cartilage calcifies due to the invasion of blood vessels and osteoprogenitor cells. This bone tissue is characterized by its disorganized collagen fibers and bone cell arrangement. This primary bone provides a temporary and provisional structure that will be remodeled into lamellar bone, a bone tissue that becomes more organized as the endochondral ossification progresses.

In this work, the remodeling process begins once the architecture of the primary trabecular bone is created through the RD equations system. It is considered a process that occurs spatially and temporally at discrete sites of the primary spongy bone, involving the resorption of mineralized tissue by osteoclastic cells, followed by the formation of new bone by osteoblasts, in a perfect biological balance, reproducing the homeostatic remodeling governed by equations (6a) and (6b), including a group of bone cells working within a BMU. The parameters used for the numerical solution of this system of equations are shown in Table 2. These parameters have proven to be suitable for giving rise to stable oscillations of the cell population and bone mass and determining the oscillation period for the constant rate of removal of osteoblasts and osteoclasts, as well as the net autocrine and paracrine regulation.

Parameter	Stable Oscillations	
X_1	11	cells
X_2	212	cells
α_1	3	cells día^{-1}
α_2	4	day^{-1}
β_1	0.2	day^{-1}
β_2	0.02	day^{-1}
k_1	0.093%	cell day^{-1}
k_2	0.008%	cell day^{-1}
g_{11}	1.1	
g_{12}	1.0	
g_{21}	-0.5	
g_{22}	0.0	

Table 2. Parameters used in the bone remodeling cycle.

The architecture of the trabecular bone obtained through the endochondral ossification model was divided into cubic elements of 0.018 mm per side. Each element on the trabecular surface is considered a potential space where Howships' lacunae can be produced during bone remodeling [46], [47]. This process was performed on the trabecular surface, simulating the occurrence of microdamage due to excessive forces or maintenance of the trabecula to preserve stable mass and adapt to mechanical stimuli. This process is illustrated in Figure 9. Initially, the highlighted areas on

the trabecular surface (zones A, B, C, D, and E in Figure 9a) represent regions where the trabecula's integrity is maintained, and subsequently, the Howships' lacunas will be created by the osteoclast cells. In these areas, the BMU's action increases the population of osteoclasts, leading to the degradation of the bone tissue due to the appearance of micro defects (Figure 9b). Subsequently, an increase in the population of osteoblastic cells initiates the mineralization process, restoring the tissue to maintain bone density on the trabecular surface. The behavior of the cell population within the BMU and the variation in bone density in the time can be observed in Figures 9c and 9d.

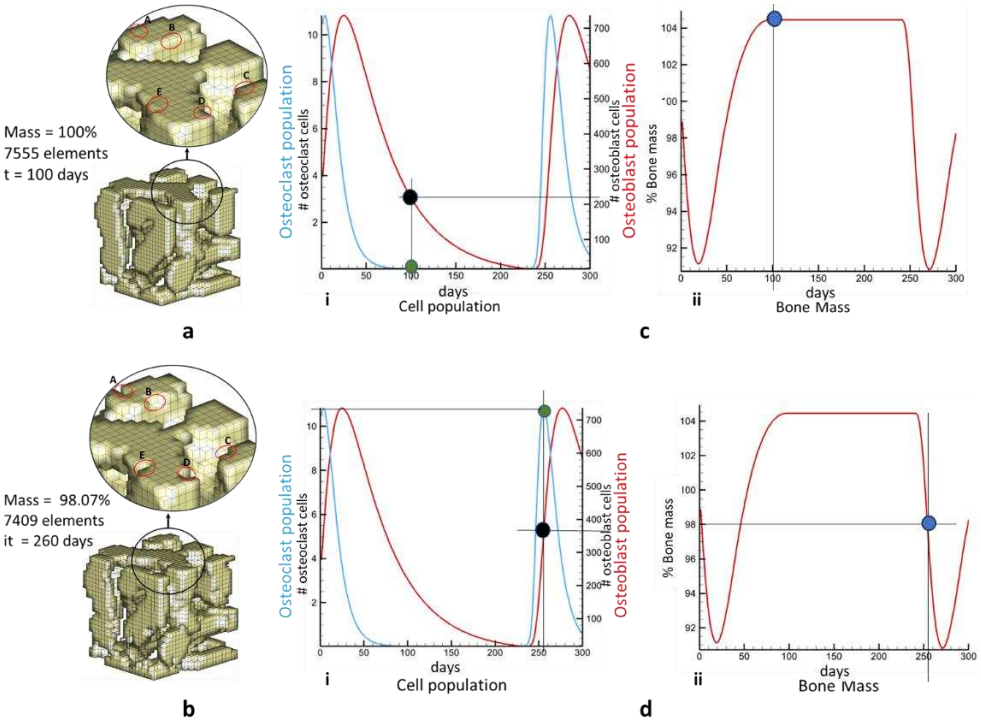

Figure 9. Population dynamics of osteoblastic and osteoclastic cells and the corresponding bone mass variation during bone remodeling over a time interval of 0 to 300 days. **a.** Configuration of the trabecular bone portion on day 100 of the remodeling cycle with 100% bone mass. Possible areas where bone resorption occurs are highlighted with red circles. **b.** Configuration of the trabecular bone portion on day 260 of the remodeling cycle with 98% bone mass. Possible areas where bone deposition occurs are highlighted with red circles. **c. i.** Graphs of the variation in the behavior of the osteoclastic cell population (blue line) and the osteoblastic cell population (red line). On day 100, there are no osteoclastic cells (green point), and the osteoblast population consists of 225 cells (black point). **ii.** Graph of bone mass variation, where the blue point indicates that on day 100, the trabecular bone portion retains 100% of its bone mass. **d. i.** Graphs of the variation in the behavior of the osteoclastic cell population (blue line) and the osteoblastic cell population (red line). On day 260, there are 12 osteoclastic cells (green point), and the osteoblast population consists of 375 cells (black point). **ii.** Graph of bone mass variation, where the blue point indicates that on day 260, the trabecular bone portion retains 98% of its bone mass.

The complete cycle of bone resorption and deposition for homeostatic remodeling and the variation in bone mass are evidenced in Figures 10 and 11, respectively. The simulation of this process was conducted for 232 days, and the resorption results are shown for days 0, 4, 16, 40, 80, and 128, with a variation in mass from 100% on day 0 to 85.5% on day 128.

The process of bone deposition, carried out by the action of osteoblasts, initiates on day 128 with a mass of 85.5%. The simulation results are presented for days 132, 140, 156, 188, and 232, again achieving 100% of bone mass. This homeostatic remodeling process occurs exclusively on the surface of trabeculae and asynchronously. Its execution depends on mechanical or maintenance demands to ensure the structural integrity of trabecular bone.

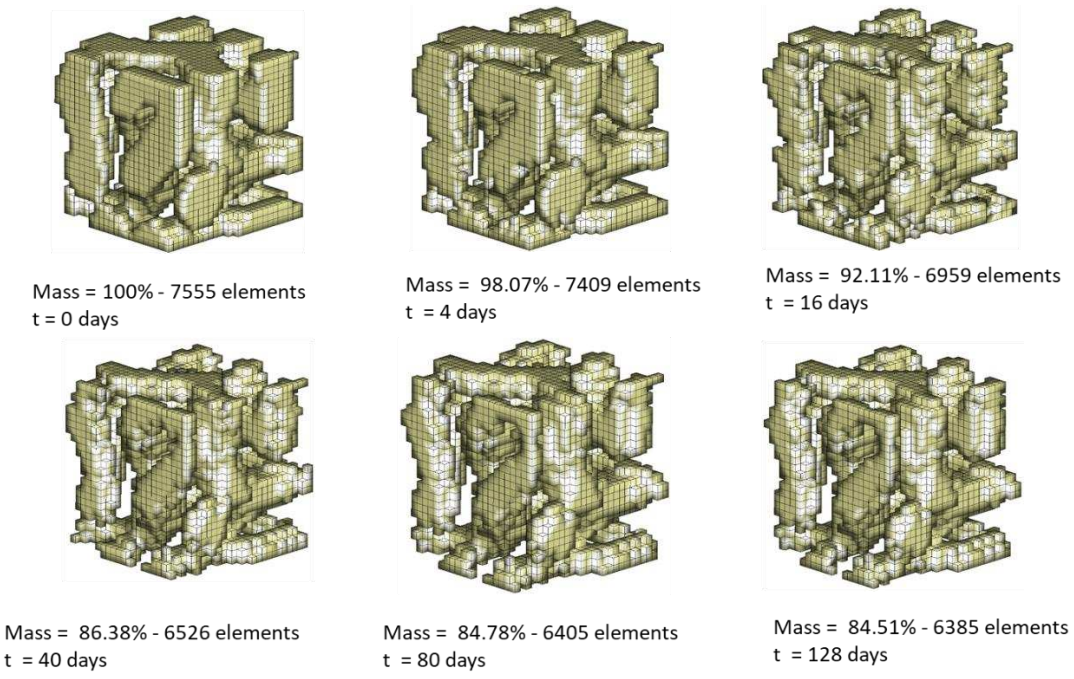

Figure 10. Schematic representation of bone resorption process over a time interval of 0 to 128 days in a cubic bone portion of 0.46 mm per side. The cycle shows a mass reduction of 15.49%

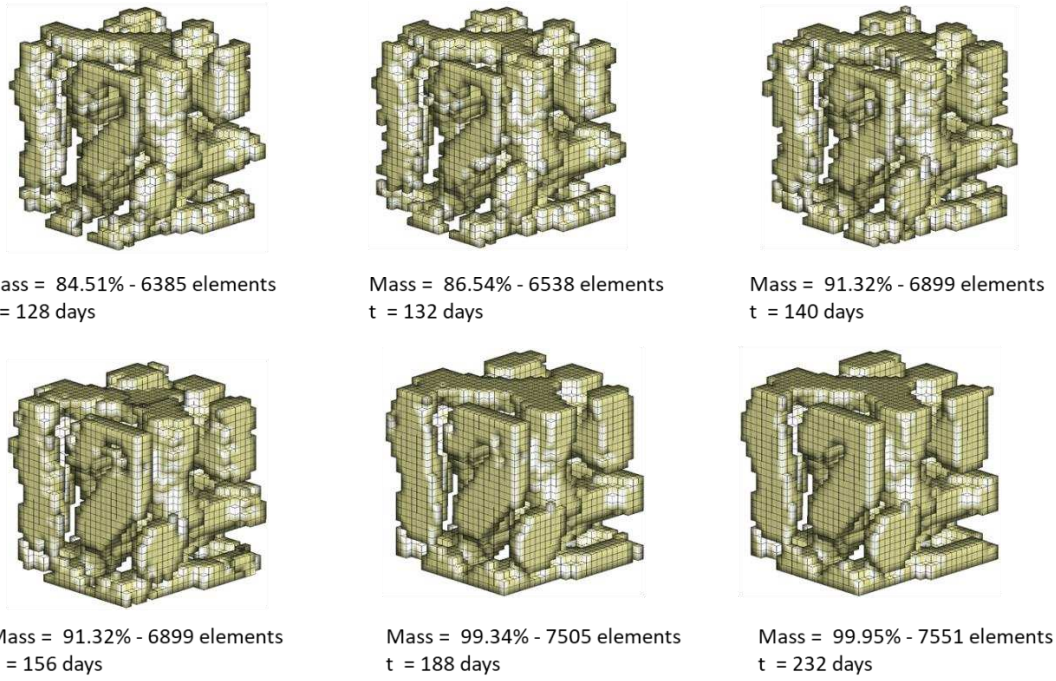

Figure 11. Schematic representation of bone formation process over a time interval of 128 to 232 days in a cubic bone portion of 0.46 mm per side. The cycle shows a complete bone mass restoration for the homeostatic remodeling process.

According to the above, the process of homeostatic remodeling in this work is governed by the model presented by Komarova et al. [35], in which bone remodeling maintains a perfect equilibrium over time within the BMU in its processes of resorption and deposition, in order to preserve bone mass through the control of population dynamics by regulating paracrine and endocrine factors released by osteoprogenitor cells.

The results of homeostatic remodeling presented in Figures 10 and 11 demonstrate the response to variations in the percentage of bone mass in a small portion of trabecular bone in perfect synchrony. However, for maintenance and turnover to occur without compromising the mechanical demands of the bone structure, a phase shift in the remodeling process is required in other areas of the bone during the same time, as depicted in Figure 12.

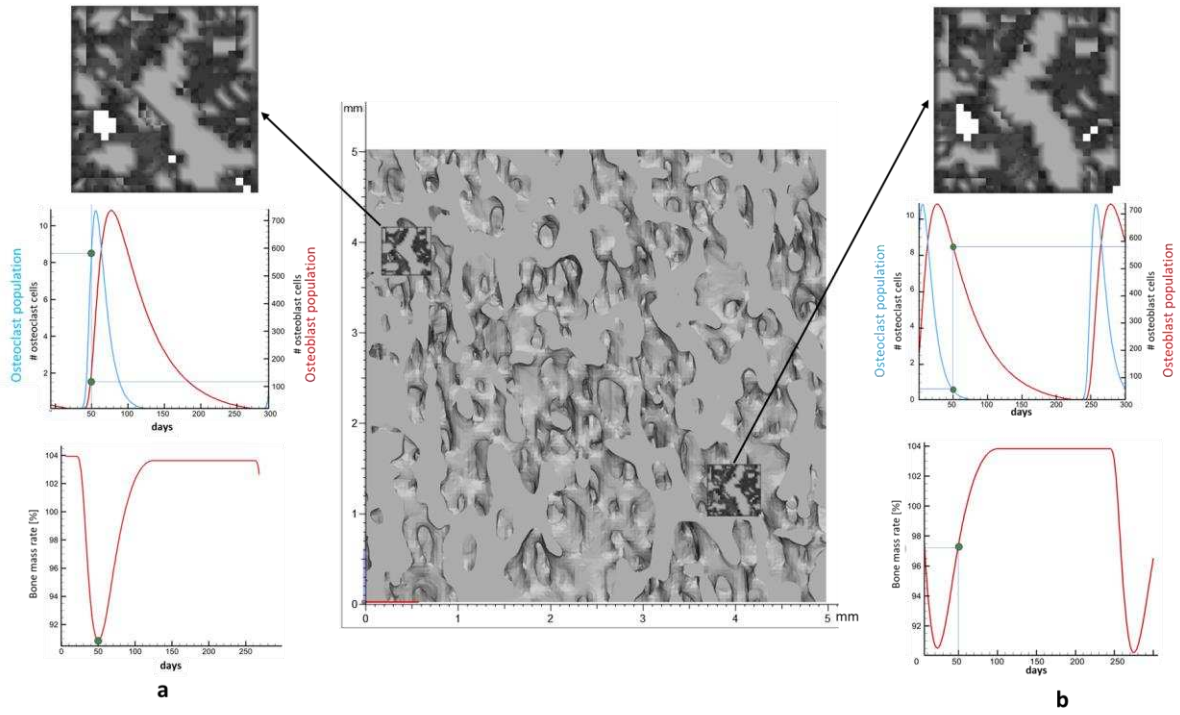

Figure 12. Bone remodeling process at two different points in a 5 mm side portion of the trabecular bone over 50 days. **a.** Bone resorption process involving cellular population dynamics and variations in bone mass. In this case, the BMU consists of approximately nine osteoclasts and 110 osteoblasts, with a bone mass rate of 91% for the trabecula. **b.** Bone deposition process involving cellular population dynamics and variations in bone mass. In this case, the BMU consists of approximately one osteoclast and 580 osteoblasts, with a bone mass rate of 96.6% for the trabecula. The green points indicate in the respective graphs the population within a BMU of osteoblasts, osteoclasts, and bone mass variation on day 50 for the trabeculae highlighted within the bone portion.

Figure 12 illustrates the asynchronous process occurring at two different points in the trabecular bone portion during remodeling within a BMU. At each point, the variation in the population of osteoblastic and osteoclastic cells for bone renewal on the trabecular surface can be observed. According to Komarova's model and the simulation conducted, at the point shown in Figure 12a and over 50 days, the cellular population in a BMU for osteoclasts increases to approximately nine cells. At the same time, osteoblasts are around 110 cells, resulting in a bone mass rate of 91%, indicating the resorption stage in the remodeling process. On the other hand, figure 12b shows an increase in bone mass, reaching 96.6% over the same 50 days, demonstrating a decrease in osteoclasts by approximately eight cells and an increase in the osteoblast population, reaching 580 cells in the BMU. The last indicates that the BMU is in the stage of bone tissue deposition.

5.0 CONCLUSION

The main objective of this article focused on bone modeling and remodeling processes. Implementing the proposed endochondral ossification model does not encompass all biological processes in bone development. Nevertheless, the central premise of this study is based on the bone formation cycle, guided by the interaction among molecular factors expressed by

chondrocytes in the growth plate, such as MMP13 and VEGF. These elements diffuse in the hyaline cartilage, subsequently interacting to generate biological patterns that give rise to the structure of trabecular bone. This work represents this interaction through a reaction-diffusion system with parameters in the Turing space and a reactive term of glycolysis, accurately reproducing the morphology observed in immature trabecular bone.

The presented model of endochondral ossification proposes a single dynamic process that plays a crucial role in both temporal and spatial self-organization of bone mineral metabolism. The convergence of temporal and spatial factors into a single dynamic process suggests an intrinsic interconnection, providing a more holistic perspective to comprehend the complexity of bone tissue formation. Therefore, the results reinforce the proposed model's validity and ability to effectively capture critical processes involved in forming trabecular bone.

The remodeling stage aims to explain the population variation process of cells in the bone tissue within a BMU for bone mass turnover and trabeculae mineralization. This process happens spatially and temporally at discrete sites, involving the resorption of mineralized tissue by osteoclastic cells, followed by the formation of new bone by osteoblasts. This process operates in a perfect biological balance in mass and time, reproducing the homeostatic remodeling governed by the model presented in equations (6).

This work presents an intrinsic connection between bone modeling and remodeling processes, which have typically been addressed separately. Firstly, it explores the development of an embryonic architecture influencing the structural adaptation of bone to mechanical demands. Secondly, it addresses the bone's mineral homeostatic function. This integrative approach reflects the essential link between the mineral stability of bone and its structural evolution, marking a significant advance in understanding these processes.

On the other hand, the results presented here open the door to more detailed investigations exploring the interplay between molecular factors in endochondral ossification and variations in population dynamics, considering the activation of paracrine and endocrine factors in bone remodeling. The above contributes to a deeper understanding of bone physiology and its long-term implications for bone health. However, although the processes presented here are framed within embryonic development and do not consider the effect of mechanical loads, their importance in bone maintenance and modeling is not disregarded. They should be considered as the primary input for understanding remodeling processes in mature stages of trabecular bone and, in this way, delving into the maintenance of bone structure and the emergence of pathologies resulting from imbalances in the production of molecular factors and variations in the population of bone cells in a BMU.

Ethics Statement

The authors have nothing to report.

6.0 REFERENCES

[1] S. M. Sadeghian, F. D. Shapiro, and S. J. Shefelbine, “Computational model of endochondral ossification: Simulating growth of a long bone,” *Bone*, vol. 153, no. May, p. 116132, 2021, doi: 10.1016/j.bone.2021.116132.

[2] E. J. Mackie, Y. a Ahmed, L. Tatarczuch, K.-S. Chen, and M. Mirams, “Endochondral ossification: how cartilage is converted into bone in the developing skeleton.,” *Int J Biochem Cell Biol*, vol. 40, no. 1, pp. 46–62, Jan. 2008, doi: 10.1016/j.biocel.2007.06.009.

[3] E. J. Mackie, Y. a Ahmed, L. Tatarczuch, K.-S. Chen, and M. Mirams, “Endochondral ossification: how cartilage is converted into bone in the developing skeleton.,” *Int J Biochem Cell Biol*, vol. 40, no. 1, pp. 46–62, Jan. 2008, doi: 10.1016/j.biocel.2007.06.009.

[4] J. E. M. Brouwers, C. C. van Donkelaar, B. G. Sengers, and R. Huiskes, “Can the growth factors PTHrP, Ihh and VEGF, together regulate the development of a long bone?,” *J Biomech*, vol. 39, no. 15, pp. 2774–82, Jan. 2006, doi: 10.1016/j.jbiomech.2005.10.004.

[5] S. Provot and E. Schipani, “Molecular mechanisms of endochondral bone development.,” *Biochem Biophys Res Commun*, vol. 328, no. 3, pp. 658–65, Mar. 2005, doi: 10.1016/j.bbrc.2004.11.068.

[6] G. V Segre and K. Lee, “Endochondral Bone Formation Regulation by Parathyroid Hormone-Related Peptide , Indian Hedgehog , and Parathyroid Hormone,” in *The Parathyroids: Basic and Clinical Concepts*, Second edi., San Diego, California: Academic Press, 2001, ch. 15, pp. 245–260.

[7] Y. Liu, B. Kuang, B. B. Rothrauff, R. S. Tuan, and H. Lin, “Robust bone regeneration through endochondral ossification of human mesenchymal stem cells within their own extracellular matrix,” *Biomaterials*, vol. 218, no. July, 2019, doi: 10.1016/j.biomaterials.2019.119336.

[8] H. F. Duncan *et al.*, “The Critical Role of MMP13 in Regulating Tooth Development and Reactionary Dentinogenesis Repair Through the Wnt Signaling Pathway,” *Front Cell Dev Biol*, vol. 10, no. April, pp. 1–21, 2022, doi: 10.3389/fcell.2022.883266.

[9] S. Bolamperti, I. Villa, and A. Rubinacci, “Bone remodeling: an operational process ensuring survival and bone mechanical competence,” Dec. 01, 2022, *Springer Nature*. doi: 10.1038/s41413-022-00219-8.

[10] M. E. Dolack *et al.*, *Computational morphogenesis of embryonic bone development: past, present, and future*. Elsevier Inc., 2019. doi: 10.1016/B978-0-12-817931-4.00011-X.

[11] K. M. Márquez-Flórez, J. R. Monaghan, S. J. Shefelbine, A. Ramirez-Martínez, and D. A. Garzón-Alvarado, “A computational model for the joint onset and development,” *J Theor Biol*, vol. 454, pp. 345–356, 2018, doi: 10.1016/j.jtbi.2018.04.015.

[12] F. J. Burgos-Flórez, M. E. Gavilán-Alfonso, and D. A. Garzón-Alvarado, “Flat bones and sutures formation in the human cranial vault during prenatal development and infancy: A computational model,” *J Theor Biol*, vol. 393, pp. 127–144, 2016, doi: 10.1016/j.jtbi.2016.01.006.

[13] H. Khayyeri and P. J. Prendergast, “The emergence of mechanoregulated endochondral ossification in evolution,” *J Biomech*, vol. 46, no. 4, pp. 731–737, 2013, doi: 10.1016/j.jbiomech.2012.11.030.

[14] E. Seeman, “Bone modeling and remodeling.,” *Critical Review in Eukaryotic Gene Expression*, vol. 19, no. 3, pp. 219–233, 2009, doi: 10.1615/critreveukargeneexpr.v19.i3.40.

[15] M. R. Allen and D. B. Burr, “Bone Modeling and Remodeling,” in *Basic and Applied Bone Biology*, Elsevier Inc., 2013, pp. 75–90. doi: 10.1016/B978-0-12-416015-6.00004-6.

[16] A. M. Turing, “The chemical basis of morphogenesis,” *Philos Trans R Soc Lond B Biol Sci*, vol. 237, no. 641, pp. 37–72, 1952, doi: 10.1098/rstb.1952.0012.

[17] O. R. López-Vaca and D. A. Garzón-Alvarado, “Spongiosa primary development: A biochemical hypothesis by turing patterns formations,” *Comput Math Methods Med*, vol. 2012, pp. 11–13, 2012, doi: 10.1155/2012/748302.

[18] K. J. Painter, “Chemotaxis as a mechanism for Morphogenesis,” College, University of Oxford, 1997.

[19] P. K. Maini, “Mathematical Models in Morphogenesis.,” in *Mathematics inspired by biology*, vol. 40, no. 4, Berlin/Heidelberg: Springer, 1999, pp. 151–189. doi: 10.2307/2531180.

[20] J. D. Murray, *Mathematical Biology I. An Introduction*, 3rd ed. Berlin: Springer, 2002.

[21] J. D. Murray, *Mathematical Biology II : Spatial Models and Biomedical Applications , Third Edition*, 3rd ed. Springer, 2003.

[22] P. K. Maini, “Using mathematical models to help understand biological pattern formation,” *C R Biol*, vol. 327, no. 3, pp. 225–234, 2004, doi: 10.1016/j.crvi.2003.05.006.

[23] J. Schnakenberg, “Simple chemical reaction systems with limit cycle behaviour,” *J Theor Biol*, vol. 81, no. 3, pp. 389–400, 1979, doi: 10.1016/0022-5193(79)90042-0.

[24] J. D. Murray, “Parameter space for turing instability in reaction diffusion mechanisms: A comparison of models,” *J Theor Biol*, vol. 98, no. 1, pp. 143–163, 1982, doi: 10.1016/0022-5193(82)90063-7.

[25] P. Blázquez-Carmona, J. Mora-Macías, A. Pajares, Á. Mármol, and E. Reina-Romo, “On the influence of structural and chemical properties on the elastic modulus of woven bone under healing,” *Front Bioeng Biotechnol*, vol. 12, Oct. 2024, doi: 10.3389/fbioe.2024.1476473.

[26] F. Shapiro and J. Y. Wu, “Woven bone overview: Structural classification based on its integral role in developmental, repair and pathological bone formation throughout vertebrate groups,” *Eur Cell Mater*, vol. 38, pp. 137–167, 2019, doi: 10.22203/eCM.v038a11.

[27] S. H. Ralston, “Bone structure and metabolism,” *Medicine*, vol. 49, no. 9, pp. 567–571, 2021, doi: https://doi.org/10.1016/j.mpmed.2021.06.009.

[28] F. Shapiro *et al.*, “Histopathology of osteogenesis imperfecta bone. Supramolecular assessment of cells and matrices in the context of woven and lamellar bone formation using light, polarization and ultrastructural microscopy,” *Bone Rep*, vol. 14, Jun. 2021, doi: 10.1016/j.bonr.2020.100734.

[29] L. Corral Gudino, “Paget’s disease of bone: 1877–2023. Etiology, and management of a disease on epidemiologic transition,” *Med Clin (Barc)*, vol. 161, pp. 207–216, 2023, doi: 10.1016/j.medcle.2023.05.010.

[30] E. F. McCarthy, “The histology of metabolic bone disease,” *Diagn Histopathol*, vol. 22, no. 10, pp. 378–383, Oct. 2016, doi: https://doi.org/10.1016/j.mpdhp.2016.09.004.

[31] D. Quexada *et al.*, “A unified framework of cell population dynamics and mechanical stimulus using a discrete approach in bone remodelling,” *Comput Methods Biomech Biomed Engin*, vol. 0, no. 0, pp. 1–13, 2022, doi: 10.1080/10255842.2022.2065201.

[32] A. Pant, E. Paul, G. L. Niebur, and A. Vahdati, “Integration of mechanics and biology in computer simulation of bone remodeling,” *Prog Biophys Mol Biol*, vol. 164, pp. 33–45, 2021, doi: 10.1016/j.pbiomolbio.2021.05.001.

[33] M. M. A. Peyroteo, J. Belinha, L. M. J. S. Dinis, and R. M. Natal Jorge, “A new biological bone remodeling in silico model combined with advanced discretization methods,” *Int J Numer Method Biomed Eng*, vol. 35, no. 6, Jun. 2019, doi: 10.1002/cnm.3196.

[34] N. Rosa, R. Simoes, F. D. Magalhães, and A. T. Marques, “From mechanical stimulus to bone formation: A review,” *Med Eng Phys*, vol. 37, no. 8, pp. 719–728, 2015, doi: 10.1016/j.medengphy.2015.05.015.

[35] S. V. Komarova, R. J. Smith, S. J. Dixon, S. M. Sims, and L. M. Wahl, “Mathematical model predicts a critical role for osteoclast autocrine regulation in the control of bone remodeling,” *Bone*, vol. 33, no. 2, pp. 206–215, 2003, doi: 10.1016/S8756-3282(03)00157-1.

[36] D. A. Garzón-Alvarado, J. M. García-Aznar, and M. Doblaré, “Appearance and location of secondary ossification centres may be explained by a reaction-diffusion mechanism.,” *Comput Biol Med*, vol. 39, no. 6, pp. 554–61, Jun. 2009, doi: 10.1016/j.compbiomed.2009.03.012.

[37] D. A. Garzón-Alvarado and A. M. Ramírez Martinez, “A biochemical hypothesis on the formation of fingerprints using a turing patterns approach.,” *Theor Biol Med Model*, vol. 8, p. 24, Jan. 2011, doi: 10.1186/1742-4682-8-24.

[38] D. A. Garzón-alvarado, “A biochemical strategy for simulation of endochondral and intramembranous ossification,” *Comput Methods Biomech Biomed Engin*, no. March 2014, pp. 37–41, 2013, doi: 10.1080/10255842.2012.741597.

[39] S. M. Sadeghian, F. D. Shapiro, and S. J. Shefelbine, “Computational model of endochondral ossification: Simulating growth of a long bone,” *Bone*, vol. 153, no. July, p. 116132, 2021, doi: 10.1016/j.bone.2021.116132.

[40] D. A. Garzón-alvarado, A. Maria, R. Martinez, D. Luis, and L. Segrera, “A model of cerebral cortex formation during fetal development using reaction – diffusion – convection equations with Turing space parameters,” *Computer Methods and Programs in Biomedicine Methods Programs Biomed.*, vol. 104, pp. 489–497, 2011, doi: 10.1016/j.cmpb.2011.07.001.

[41] D. Patra, E. DeLassus, S. Hayashi, and L. J. Sandell, “Site-1 protease is essential to growth plate maintenance and is a critical regulator of chondrocyte hypertrophic differentiation in postnatal mice,” *Journal of Biological Chemistry*, vol. 286, no. 33, pp. 29227–29240, Aug. 2011, doi: 10.1074/jbc.M110.208686.

[42] J. J. Dibner, J. D. Richards, M. L. Kitchell, and M. A. Quiroz, “Metabolic Challenges and Early Bone Development,” *Journal of Applied Poultry Research*, vol. 16, no. 1, pp. 126–137, 2007, doi: https://doi.org/10.1093/japr/16.1.126.

[43] K. Huch, S. Kleffner, J. Stöve, W. Puhl, K.-P. Günther, and R. E. Brenner, “PTHrP, PTHr, and FGFR3 are involved in the process of endochondral ossification in human osteophytes.,” *Histochem Cell Biol*, vol. 119, no. 4, pp. 281–7, Apr. 2003, doi: 10.1007/s00418-003-0519-2.

[44] L. Wang, Y. Y. Shao, and R. T. Ballock, “Thyroid hormone-mediated growth and differentiation of growth plate chondrocytes involves IGF-1 modulation of beta-catenin signaling.,” May 2010. doi: 10.1002/jbmr.5.

[45] X. Yang and G. Karsenty, “Transcription factors in bone: developmental and pathological aspects,” *Trends Mol Med*, vol. 8, no. 7, pp. 340–345, 2002.

[46] V. Everts, I. D. C. Jansen, and T. J. de Vries, “Mechanisms of bone resorption,” *Bone*, vol. 163, Oct. 2022, doi: 10.1016/j.bone.2022.116499.

[47] T. Hefti, M. Frischherz, N. D. Spencer, H. Hall, and F. Schlottig, “A comparison of osteoclast resorption pits on bone with titanium and zirconia surfaces,” *Biomaterials*, vol. 31, no. 28, pp. 7321–7331, Oct. 2010, doi: 10.1016/j.biomaterials.2010.06.009.